

# Dynamics of a Single Peak of the Rosensweig Instability in a Magnetic Fluid

Adrian Lange<sup>1</sup>, Heinz Langer, Andreas Engel

*Institut für Theoretische Physik, Otto-von-Guericke-Universität, PF 4120,  
D-39016 Magdeburg, Germany*

---

## Abstract

To describe the dynamics of a single peak of the Rosensweig instability a model is proposed which approximates the peak by a half-ellipsoid atop a layer of magnetic fluid. The resulting nonlinear equation for the height of the peak leads to the correct subcritical character of the bifurcation for static induction. For a time-dependent induction the effects of inertia and damping are incorporated. The results of the model show qualitative agreement with the experimental findings, as in the appearance of period doubling, trebling, and higher multiples of the driving period. Furthermore a quantitative agreement is also found for the parameter ranges of frequency and induction in which these phenomena occur.

*PACS:* 47.20.Ma; 75.50.Mm; 05.45.-a

*Key words:* Interfacial instability; Magnetic liquids; Nonlinear dynamics and nonlinear dynamical systems

---

## 1 Introduction

Magnetic fluids (MF) are stable colloidal suspensions of ferromagnetic nanoparticles (typically magnetite or cobalt) dispersed in a carrier liquid (typically oil or water). The nanoparticles are coated with a layer of chemically adsorbed surfactants to avoid agglomeration. The behaviour of MF is characterized by the complex interaction of their hydrodynamic and magnetic properties with external forces. Magnetic fluids have a wide range of applications [1] and show many fascinating effects [2], as the labyrinthine instability or the Rosensweig instability. The latter instability occurs when a layer of MF with a free surface

---

<sup>1</sup> Corresponding author.

E-mail: adrian.lange@physik.uni-magdeburg.de.

is subjected to a uniform and vertically oriented magnetic field. Above a certain threshold of the magnetic field that surface becomes unstable, giving rise to a hexagonal pattern of peaks [3]. Superimposing the static magnetic field with oscillating external forces leads to nonlinear surface oscillations. Experimentally, either vertical vibrations [4–6] or magnetic fields [7–11] have been investigated as alternating external forces.

For free surface phenomena the fluid motion strongly depends on the shape of the surface and vice versa. Additionally for MF, the shape of the surface is determined by the magnetic field configuration which contributes via the Kelvin force to the Navier-Stokes equation the solution of which gives the flow field. Thus the dynamics of MF is inherently governed by the nonlinear interaction between the flow field, the surface shape, and the magnetic field configuration.

For that reason one attempts to study simple systems of MF which nevertheless show the essential features. The nonlinear dynamics of a single peak of magnetic fluid, i.e., the dynamics of a 0-dimensional system in a vertically oscillating magnetic field was studied exemplarily in [10]. By varying the amplitude and the frequency of the alternating field and the strength of the static field, the peak response can be harmonic, subharmonic (twice the driving period) or higher multiples of the driving period. For suitable choices of the parameters, non-periodic chaotic peak oscillations were observed.

Taking the above described circumstances into account for a theoretical approach, a sound model should be analytically tractable as well as capable of showing all essential features. Beyond these primary demands, the model may also predict new phenomena of peak oscillations. The aspiration to confirm such new phenomena experimentally motivates a simple and robust model to guide the design of the experimental setup.

Such a model is proposed for the dynamics of a single peak of MF. It is based on the approximation of the peak by a half-ellipsoid with the same height and radius as the peak. The resulting equation giving the dependence of the height of the peak on the applied induction is derived in the following section. The character of the bifurcation is analysed in Sec. III for the case of a static induction. In Sec. IV the dynamics of the peak is studied and the results are compared with the experimental behaviour for different frequencies of a time-dependent induction. The final section summarizes the results and outlines two aspects for further experiments.

## 2 Model

The complex and nonlinear interactions in MF with a free surface formed by a peak (see Fig. 1) present a formidable problem, since the form of the peak is not known analytically. The aim of our model is an analytical equation for the height of the peak at its centre  $\mathbf{r} = (x, y) = 0$ . The shape of the peak, particular the form at the tip of the peak is beyond the potential of this model. The equation will thus neglect the influence of the surface regions away from the peak tip and of the boundaries.

A layer of an incompressible, nonconducting, and inviscid MF of half-infinite thickness between  $z = 0$  and  $z \rightarrow -\infty$  is considered with a free surface described by  $z = \zeta(x, y, t)$ . It is assumed that the magnetization  $\mathbf{M}$  of the MF depends linearly on the applied magnetic field  $\mathbf{H}$ ,  $\mathbf{M} = \chi\mathbf{H}$ , where  $\chi$  is the susceptibility of the MF. The system is governed by the equation of continuity,  $\text{div } \mathbf{v} = 0$ , and the Euler equation for MF in the presence of gravity

$$\rho [\partial_t \mathbf{v} + (\mathbf{v} \text{ grad}) \mathbf{v}] = -\text{grad } p + \mu_0 M \text{ grad } H + \rho \mathbf{g}, \quad (1)$$

where the magnetostriction is neglected and the co-linearity of the magnetization and the field is exploited for the magnetic force term. In Eq. (1) the velocity field is denoted by  $\mathbf{v}$ , the density of the MF by  $\rho$ , the pressure by  $p$ , the permeability of free space by  $\mu_0$  and the acceleration due to gravity by  $\mathbf{g}$ .  $M$ ,  $H$ , and  $B$  are the absolute values of the magnetization, the magnetic field and the induction  $\mathbf{B}$  in the fluid. In the static case,  $\mathbf{v} = 0$ , the integral of the equation of motion (1) may be calculated to give

$$p = -\rho g z + \mu_0 \int_0^H M dH' + \text{const}. \quad (2)$$

The remaining boundary condition in the static case, the continuity of the normal stress across the free surface, gives

$$p = \sigma K - \frac{\mu_0}{2} (\mathbf{M} \mathbf{n})^2 \quad \text{at } z = \zeta, \quad (3)$$

where the pressure in the non-magnetic medium above the MF was set to zero. The surface tension between the magnetic and non-magnetic medium is denoted by  $\sigma$ , the curvature of the surface by  $K = \text{div } \mathbf{n}$ , and the unit vector normal to the surface by  $\mathbf{n}$ . By inserting Eq. (2) at  $z = \zeta$  into Eq. (3), the

balance of pressure results in an equation for the surface  $\zeta$

$$\rho g \zeta - \mu_0 \left( \frac{M_n^2}{2} + \int_0^{H(\zeta)} M dH' \right) + \sigma K = \text{const} \quad (4)$$

with  $M_n = \mathbf{M} \cdot \mathbf{n}$ . After the peak is formed, the equilibrium is characterized by the equality of the pressure along the surface. Motivated by our aim of an analytically tractable model, we choose the two reference points  $\mathbf{r} = 0$ , the centre of the peak, and  $|\mathbf{r}| \gg 0$ , the flat interface far away from the peak, where the pressure equality is evaluated. The magnetization is related to the induction by

$$M = \frac{\chi}{\mu_0(\chi + 1)} B(\mathbf{r}). \quad (5)$$

Applying Eq. (4) at  $(\mathbf{r} = 0, \zeta = h)$  and  $(|\mathbf{r}| \gg 0, \zeta = 0)$  leads to

$$-\rho g h - \sigma K(h) + \frac{\chi}{2\mu_0(\chi + 1)} B_{ext}^2 \left\{ \left[ \frac{B(h)}{B_{ext}} \right]^2 - 1 \right\} = 0, \quad (6)$$

where  $B_{ext}$  is the external applied induction. The remaining two unknown quantities, the curvature  $K(h)$  and the induction  $B(h)$  at the tip of the peak, are determined by an approximation. We model the peak, which is assumed to be rotationally symmetric, by a half-ellipsoid with the same height and radius as the peak (see Fig. 1). Thus one can make use of the analytical results for a rotational ellipsoid with the vertical (horizontal) semiprincipal axis  $h$  ( $R$ ) with the curvature given by

$$K \Big|_{z=h} = \frac{h}{R^2} \quad (7)$$

and the induction [12]

$$B \Big|_{z=h} = B_{ell} = \frac{\chi + 1}{1 + \chi \beta} B_{ext} \quad \text{with} \quad (8)$$

$$\beta = \begin{cases} \frac{1 + \epsilon^2}{\epsilon^3} (\epsilon - \arctan \epsilon) & \epsilon = \sqrt{(R/h)^2 - 1} \quad \text{for } R > h \\ \frac{1 - \epsilon^2}{\epsilon^3} (\text{artanh } \epsilon - \epsilon) & \epsilon = \sqrt{1 - (R/h)^2} \quad \text{for } R < h. \end{cases} \quad (9)$$

It is emphasized that an applied induction  $B_{ext}$  results in a uniform induction  $B_{ell}$  within the ellipsoid. The demagnetization factor  $\beta$  is a purely geometrical quantity because it relates the dimensions of the major and minor semiprincipal axes by means of the eccentricity  $\epsilon$ . Whereas (7) can be substituted directly into Eq. (6), the result (8) has to be modified to the case of a half-ellipsoid atop the layer of MF. The proposed modification is

$$B \Big|_{z=h} = \frac{1 + \chi(1 + \lambda\beta)}{1 + \chi\beta(1 + \lambda\beta)} B_{ext}, \quad (10)$$

where a parameter  $\lambda$  is introduced, which mimics the influence of the magnetic field of the layer on the field at the tip of the peak. The form of (10) ensures that in the limits of a magnetically impermeable material ( $\chi = 0$ ), of a ‘magnetic conductor’ ( $\chi \rightarrow \infty$ ), of a very oblate ellipsoid ( $\beta \simeq 1$ ), and of a very prolate ellipsoid ( $\beta \simeq 0$ ) the results are the same as in Eq. (8). As long as the height of the half-ellipsoid is large compared to its diameter, the influence of the magnetic layer on the magnetic field at the tip of the peak is small. This is obviously not the case if the half-ellipsoid becomes disk-shaped, i.e.  $h < R$ . For this case (10) is expanded up to the first order in  $h/R$ ,

$$B \Big|_{z=h, h \ll R} \simeq \left[ 1 + \frac{\chi(1 + \lambda)\pi h}{[1 + \chi(1 + \lambda)]2R} \right] B_{ext} \quad (11)$$

and compared to the analytical result for  $B$  at the crest of a sinusoidal surface wave (SW) (pp. 178 in [2]) with the wave length  $4R$  (Fig. 2)

$$B \Big|_{z=h, SW} = \left[ 1 + \frac{\chi\pi h}{(\chi + 2)2R} \right] B_{ext}. \quad (12)$$

The condition that both values of  $B$  should coincide, leads to an equation for the parameter  $\lambda$

$$\lambda = -\frac{1}{2}. \quad (13)$$

The determination of  $\lambda$  adjusts the radius, since the critical wave number for surface waves is the capillary wave number,  $k_c = (2\pi/\lambda_c) = \sqrt{\rho g/\sigma}$ . Therefore the radius of the half-ellipsoid is fixed to  $R = (\lambda_c/4) = \pi/(2k_c)$ . By inserting (7) into (6) and introducing dimensionless quantities for all lengths and the induction

$$\bar{h} = \sqrt{\frac{\rho g}{\sigma}} h \quad \bar{B} = \frac{\chi}{\sqrt{2\mu_0(\chi + 1)(\chi + 2)\sqrt{\rho\sigma g}}} B \quad (14)$$

we obtain a *nonlinear* equation for the dependence of the peak height  $\bar{h}$  on the applied induction  $\bar{B}_{ext}$  (the bars are omitted for the rest of the paper)

$$B_{ext}^2 \left[ \left( \frac{B(h)}{B_{ext}} \right)^2 - 1 \right] - h \left[ 1 + \frac{1}{R^2} \right] \frac{\chi}{(\chi + 2)} = 0. \quad (15)$$

The nonlinear behaviour enters into the equation through  $B(h)/B_{ext}$  which is determined by (9, 10, 13). Eq. (15) presents the fundamental equation of the model in which the height of the peak depends on the properties of the applied induction only. The quality of the approximation is tested in the static case for which (15) was derived. It forms the starting point for the description of the peak dynamics, where the effects of inertia and damping have to be taken into account.

### 3 Static Peak

For a layer of MF with a free surface subjected to a vertical magnetic field there are three different energies which contribute to the total energy  $E_{tot}$ . The potential energy and the surface energy increase  $E_{tot}$  with increasing  $h$ , whereas the magnetic field energy decreases  $E_{tot}$  with increasing  $h$ . The plane surface corresponds to a minimum of the total energy at  $h = 0$ . If the surface is perturbed, the magnetic flux is concentrated in the peaks of the disturbances. The resulting force tends to increase the modulations, while surface tension and gravitational forces tend to decrease the disturbances. When the increasing field passes a certain strength  $H_c$ , the destabilizing force will win over the stabilizing ones. The resulting peaks are energetically favourable because for  $H > H_c$  the total energy has now a second minimum at  $h > 0$  which is deeper than the first one at  $h = 0$ . The transition from the first to the second minimum corresponds to the sudden jump from  $h = 0$  to  $h > 0$ . If the peaks are established, a decreasing field results in smaller heights of the peak up to a second critical field  $H_s$ , the saddle-node field, where the peaks suddenly break down. With respect to the total energy this means a transition back to the first minimum at  $h = 0$  because it is now energetically more favourable.

Such a dependence of the height of the peak on the variation of the magnetic field is typified as a hysteresis. The difference between the two critical fields defines the width of the hysteresis. For a MF with  $\chi = 1.15$  the width was measured to 6% of the critical field and the critical height at  $H_c$  is given by 2.1 mm [10]. The corresponding critical inductions are  $B_c = \mu_0[H_c + M(H_c)]$  and  $B_s = \mu_0[H_s + M(H_s)]$ .

For a static induction,  $B_{ext} = B_0$ , the solution of Eq. (15) is determined for two

susceptibilities,  $\chi = 1.15$  and  $\chi = 2.5$ . The former value is given in [10] for a mixture of EMG 901 and EMG 909 (both Ferrofluidics Corporation) in a ratio of 7 to 3, whereas the latter value was measured in a recent experiment for the same mixture [13]. For both susceptibilities a distinct hysteresis appears, whose width increases with increasing susceptibility. Correspondingly, in the limit  $\chi \rightarrow 0$  the hysteresis disappears (Fig. 3a). For  $\chi = 1.15$  the width is 5% of the critical induction  $B_c$  and the critical height of the peak is  $h_c \simeq 2.0/k_c \simeq 2.9$  mm. The material parameters  $\rho = 1377 \text{ kg m}^{-3}$  and  $\sigma = 2.86 \cdot 10^{-2} \text{ kg s}^{-2}$  as given in [10] were used. For the other chosen susceptibility,  $\chi = 2.5$ , the width is 13% of the critical induction  $B_c$  and the critical height is  $h_c \simeq 6.9/k_c \simeq 10.0$  mm.

Figure 3b shows the dependence of the width of the hysteresis on the susceptibility of the magnetic fluid. Whereas for small susceptibilities a fair increase of the width can be detected, a tendency towards a saturation in the growth can be seen for larger susceptibilities. No systematic measurements of the width of the hysteresis have yet been undertaken. Therefore any experimental test which would determine the range of validity of the model is pending on subsequent measurements.

Despite the simplicity of the proposed approximation, the model describes the generic static behaviour of the height of the peak very well, i.e. the appearance of a hysteresis for increasing and decreasing induction at nonzero susceptibilities as it is observed in experiments [10,14,15]. Note in this connection that for  $\lambda = 0$ , i.e. when neglecting the difference in the magnetic field of an ellipsoid and a half-ellipsoid, no hysteresis is found. Note also that in a one-dimensional system one finds a *supercritical* bifurcation for  $\chi < 2.53$  [16,17] whereas our simplified two-dimensional model yields a subcritical bifurcation for all values of  $\chi$  in accordance with experiment. Beyond the qualitative agreement, the quantitative values for the width of the hysteresis and the critical height are in satisfying agreement with the measurements in [10] for  $\chi = 1.15$ . This agreement is achieved without any fit-parameter since the fixed value of the parameter  $\lambda$  applies for any MF.

The fact that the critical induction is not equal to one (cf. 15) is a consequence of the evaluation of the introduced parameter  $\lambda$ , which determines the radius. The imposed value of the radius ensures the equality of the magnetic induction at the top of the oblate ellipsoid and the crest of the surface wave. But the curvature is different:  $h/R^2$  at the top of the ellipsoid is smaller than the value  $\pi^2 h/(4R^2)$  it takes at the crest of the surface wave. Thus the expansion of (15) for small  $h$  with  $R = \pi/2$

$$h \left[ B_0^2 \frac{\pi}{R} - 1 - \frac{1}{R^2} \right] = 0 \quad (16)$$

leads to a critical induction smaller than 1,  $B_c = \sqrt{1/2 + 2/\pi^2} \simeq 0.84$ . The half-ellipsoid approximation (10) with  $\lambda = -1/2$  was quantitatively compared to a numerically exact determination of the magnetic field of a rotational half-ellipsoid atop of a horizontal layer by solving the Laplace equation for the magnetic potential (Fig. 4). For  $0.5 \leq h/R \leq 6.5$  the magnetic induction at the tip of the peak is approximated with an accuracy of 1.7%. The comparison shows that the modification of the magnetic field at the tip of the peak through the magnetic field of the layer is rather weak even for small heights. This supports our assumption that the field at the tip of the peak is the essential feature to describe its behaviour.

Therefore Eq. (10) describes  $B$  directly at the height of the peak fairly accurately. Furthermore, equation (15) leads to the correct character of the bifurcation, i.e. a subcritical instability, and gives the right width of the hysteresis compared with the experimental results [10]. With this level of confirmation, the dynamics of a single peak of MF is studied in the following section.

## 4 Oscillating Peak

### 4.1 Inertia and Damping

The induction is chosen to be a superposition of a static part,  $B_0$ , and a time-dependent part,  $\Delta B \cos(\omega t)$ . The amplitude of the oscillating part is denoted by  $\Delta B$  and the frequency by  $\omega = 2\pi f = 2\pi/T$ . In correspondence with the experiments [10], the response-period of the peak is studied in dependence on the three parameters, the strength of the static part, the amplitude of the alternating part, and the driving frequency. If the last two parameters are kept constant, one distinguishes between three different regimes for the behaviour of  $h(t)$  with increasing  $B_0$ . For small  $B_0$  the surface remains flat, i.e.  $h(t) \equiv 0$ . Beyond a first, lower threshold  $h(t)$  oscillates between zero and a maximum  $h_{max}$  whereas beyond a second, higher threshold it alternates between two positive extrema,  $0 < h_{min} < h_{max}$  (see Fig. 5). The behaviour in the second regime will be the focus of our study since it was analysed experimentally in detail in [10].

In order to formulate a differential equation for the peak dynamics, the effects of inertia and damping have to be incorporated into Eq. (15). Since each term in (15) stems from the equation of pressure balance, the inertial term may be written as

$$\frac{\text{force}}{\text{area}} = \frac{m}{A} \frac{d^2 h}{dt^2} \sim \frac{\rho |h| A}{A} \frac{d^2 h}{dt^2} = \rho |h| \frac{d^2 h}{dt^2}. \quad (17)$$

The sign of proportionality indicates that in the frame of our model the mass and the area of the peak cannot be precisely determined. For these quantities the knowledge of the complete surface and the flow field are necessary. For this reason we choose the simple relation of a linear dependence of the mass of the peak on its height.

The implementation of the damping is difficult. In the experiment one observes that the peak periodically arises up to a maximal height and collapses to zero height. This behaviour leads to the assumption that the system is endowed with a dissipation mechanism which acts particularly strongly when the collapsing peak approaches  $z = 0$ . Since such a mechanism cannot be derived in the frame of the present model, the idea of an impact oscillator [19,20] is used. The impact oscillator is an externally excited oscillator, where the oscillating mass impacts on a fixed boundary. From this boundary the mass is reflected with a velocity

$$\left. \frac{dh}{dt} \right|_{t_{0+}} = -\tau \left. \frac{dh}{dt} \right|_{t_{0-}}, \quad (18)$$

where  $\tau$  is the coefficient of restitution and  $t_0$  is the time of the impact,  $h(t_0) = 0$ . Consequently, there are oscillations between  $0 \leq h < \infty$  only. For a weakly damped impact oscillator it is known [19] that infinite series of transitions from period 1 to period  $N$  ( $N = 3, 4, \dots$ ) can appear. This phenomenological resemblance to the observations in [10] also motivates the use of the idea of an impact oscillator. It is emphasized that the chosen special form of damping applies only to the second regime, where  $h(t)$  oscillates between zero and a maximum  $h_{max}$ .

In our model an impact with  $z = 0$  occurs whenever  $h(t)$  reaches zero. The height and the velocity after the impact are fixed and independent of the behaviour before the impact. We choose

$$h = 10^{-6} \quad \text{and} \quad \left. \frac{dh}{dt} \right|_{t_{0+}} = 0 \quad \text{at} \quad t = t_{0+}, \quad (19)$$

which corresponds to a nearly complete dissipation of the energy at every impact. A similar choice was made for a model proposed in [10]. The choice of fixed values is obviously an oversimplification because it does not make any difference whether a large peak with a high velocity rushes towards  $z = 0$  or whether a small peak slowly approaches  $z = 0$ .

The resulting differential equation for this cut-off mechanism in dimensionless

quantities is (the time is scaled by  $g^{3/4}\rho^{1/4}\sigma^{-1/4}$ )

$$\frac{d^2h}{dt^2} = \frac{B_{ext}^2}{h} \left[ \left( \frac{B(h)}{B_{ext}} \right)^2 - 1 \right] \frac{(\chi + 2)}{\chi} - 1 - \frac{1}{R^2} \quad (20)$$

with  $B_{ext} = B_0 + \Delta B \cos(\omega t)$ . Eq. (20) is solved by means of the forth-order Runge-Kutta integration method with a standard time step of  $T/200000$ . The other standard parameters for the integration are  $h(0) = 10^{-6}$  and  $d_t h(0) = 0$  as initial conditions and a total time of  $200T$  over which the solution is calculated. The first 100 periods are considered as transient time for the system to relax to a response-behaviour independent of the initial conditions. The last 100 periods are analysed with respect to a periodic behaviour of  $h(t)$  by means of a Poincaré section. For our one-dimensional dynamics a Poincaré section means to compare  $h$  at a certain time, say  $t_m = mT$ , with  $h$  at times, which are  $N$  periods ( $N = 1, 2, \dots$ ) later with respect to  $t_m$ :

$$\begin{aligned} h(t_m) &\stackrel{?}{=} h(t_m + T) \\ h(t_m) &\stackrel{?}{=} h(t_m + 2T) \\ &\dots \\ h(t_m) &\stackrel{?}{=} h(t_m + NT). \end{aligned} \quad (21)$$

Those equations which are fulfilled give the period  $N$  (and any higher multiples of  $N$ ) of the peak response. The chosen 100 periods of analysis ensure a good reliability of the estimated periods up to 30.

## 4.2 Results and Discussion

The results of the Poincaré sections are plotted as period diagrams in the  $B_0$ - $\Delta B$  plane at a fixed frequency  $f$  and for two different susceptibilities (see Figs. 6, 7, 9). The constant part,  $B_0$ , is sampled in steps of 0.01. The amplitude of the alternating part,  $\Delta B$ , is increased in steps of 0.025 with an initial value of 0.05. The different periods in the interesting second regime,  $0 \leq h(t) \leq h_{max}$ , are coded by colours. The periods 1 to 10 are encoded by a chart of distinctive colours starting with green, red, blue, and ending with orange. The higher periods from 11 to 30 are encoded by a continuous colour chart. Periods above 30 or a non-periodic behaviour of  $h(t)$  are noted by grey. This selection of colours is guided by the choice of colours in [10]. White areas inside and right of the coloured horizontal stripes indicate regions, where  $h(t)$  oscillates between two positive extrema. White areas left of the coloured stripes denote the regime  $h(t) \equiv 0$ .

The period diagram for a low frequency of  $f = 0.03$  ( $\simeq 2.5$  Hz) is displayed in Fig. 6. In accordance with the experimental results for 2.5 Hz (see Fig. 5a in [10]) the response of the peak is harmonic almost everywhere in the  $B_0$ - $\Delta B$  plane. Responses with higher periods are detected only at the edge towards the third regime. The area of harmonic response is cone-like shaped, where the limit to the left is given by  $\Delta B = B_c - B_0$  for  $B_0 \leq B_c$  (solid line) and the limit to the right is given by  $\Delta B = B_0 - B_c$  for  $B_0 \geq B_c$  (dashed line). These strict limits apply particularly to the MF with  $\chi = 2.5$  (Fig. 6b), whereas the right limit is more frayed for the MF with  $\chi = 1.15$  (Fig. 6a). The feature of a cone-like shape is also found in the experiment, but with a slight asymmetry at very small amplitudes of the alternating field. An asymmetry could not be found with our simple model. Another difference is that our right limit is too large compared to the experimental data.

The appearance of only harmonic responses is caused by the low frequency. The corresponding characteristic time of the excitation,  $T$ , is large enough for the peak to follow the slow modulations of the external field. Therefore the peak oscillates with the same frequency as the external excitation. By considering the quasi-static limit  $f \rightarrow 0$  (see Fig. 3), the boundaries of the second regime can be understood as follows: As long as  $B_0$  is smaller than  $B_c - \Delta B$ , the resulting external induction varies over a range where at its lower bound  $h_1 = 0$  is stable. At its upper bound either  $h_2 = 0$  is stable if  $B_0 + \Delta B < B_s$ , or  $h_2 = 0$  and  $h_2 > 0$  are stable if  $B_0 + \Delta B > B_s$ . Because of the greater attraction of zero height in the bistable area due to the strong damping at  $h = 0$ , the dynamics of  $h(t)$  is bounded by zero in both cases. If  $B_0$  is larger than  $B_c + \Delta B$ , the resulting external induction varies over a range where at its lower bound  $h_1 > 0$  is stable and at its upper bound  $h_2 > h_1$  is stable. Thus the dynamics of  $h(t)$  is bounded between  $h_1$  and  $h_2$ . Consequently, for low frequencies the peak alternates in the second regime as long as  $B_c - \Delta B \leq B_0 \leq B_c + \Delta B$ . The fact that  $h(t)$  remains at zero even when for a certain time a nonzero height is stable (but not attractive enough to win over  $h = 0$ ) was observed in the experiment, too. In our dynamics the zero height is always more attractive than the nonzero height. This is not the case in the experiment, which explains the observed lower limit to the right.

Fig. 7 shows the results for a medium frequency of  $f = 0.1$  ( $\simeq 8.2$  Hz). For the MF with the low susceptibility of  $\chi = 1.15$ , the second regime splits into two disjoint parts. For smaller values of  $B_0$  we find only harmonic responses, whereas for higher values of  $B_0$  we observe the period  $N = 2$ . The second regime is separated from the first regime by  $\Delta B = B_c - B_0$  for  $B_0 \leq B_c$  (solid line). The limit to the right is given by  $\Delta B = B_0 - B_c$  for  $B_0 \geq B_c$  (dashed line) only for amplitudes  $\Delta B$  above 0.15 (Fig. 7a). For the MF with the high susceptibility of  $\chi = 2.5$ , the second regime forms a compact region, which is separated from the first regime by  $\Delta B = B_c - B_0$  for  $B_0 \leq B_c$  (solid line). In contrast to the low frequency behaviour, the whole structure

of periods shows a specific composition. For a fixed amplitude  $\Delta B$  the peak starts to oscillate harmonically. For  $\Delta B > 0.25$  and increasing  $B_0$  the period-1 state is replaced by the period-2 state which lasts up to the right limit of the second regime. This clear two-state picture changes if  $\Delta B$  is decreased. For  $\Delta B \leq 0.25$  a tongue of high periodic ( $N > 2$ ) and non-period oscillations appears (Fig. 7b). For  $0.175 \leq \Delta B \leq 0.25$  the tongue is embedded in the period-2 state. For  $\Delta B < 0.175$  the tongue follows directly the harmonic oscillations. In this tongue we find odd-number periods of 3, 5, and 9 and even-number periods of 4, 8, 14, 16, and 18 (see Fig. 8).

The structure of periods in Fig. 7b displays generic features which are also observed in the experiment for 12.5 Hz (see Fig. 6a in [10]). Beside the agreement in the generic features, there are three major quantitative differences. The period-2 state area between the harmonic response and the tongue is much thinner than in the experiment. An extended area of period  $N = 3$  could not be found and the right limit of the period-2 state is too low compared to the experimental results.

For a frequency of  $f = 0.2$  ( $\simeq 16.4$  Hz) the results are shown in Fig. 9. For a low susceptibility of  $\chi = 1.15$  the peak starts to oscillate harmonically independently of the strength of  $\Delta B$ . With increasing  $B_0$  the period-1 state is followed by a period of  $N = 4$  for  $\Delta B \leq 0.125$ . For  $\Delta B > 0.125$  the harmonic response is mainly replaced by the period-2 state, which is then replaced by the period 3. One notes the appearance of oscillations between two positive extrema inside the second regime for the low susceptibility case (Fig. 9a). For a high susceptibility of  $\chi = 2.5$  the whole period diagram displays a band-like structure (Fig. 9b). For a fixed amplitude  $\Delta B$  and increasing  $B_0$ , the period  $N = 1$  appears first. Then either the period  $N = 6$  follows for  $\Delta B \leq 0.15$  or the periods  $N = 2$  and  $N = 6$  follow for  $\Delta B > 0.15$ . The whole structure of periodic orbits ends with a broad band of period  $N = 5$ . This last *novel* feature is remarkable because no similar phenomenon has been observed in the experiment. For all tested frequencies in [10], the second regime gives way to the third regime by a period of  $N = 1$  or  $N = 2$ .

The comparison between the experimental and theoretical data generally shows a qualitative and partly a quantitative agreement with the dynamics of the peak. This agreement is achieved with a certain choice for the mass of the peak (17) and for the strength of the impact (19). The shown results are robust against modifications of (17, 19) by a constant of  $O(1)$ . It is not necessary to fit parameters as the damping constant, the driving period, the critical field, and the resolution limit of the height in contrast to the minimal model in [10]. The other improvements are a more realistic nonlinear force term and the multiplicative character of the driving. Our results at low and medium frequencies for  $\chi = 2.5$  support the presumption that the MF used for the measurements of the dynamical behaviour has a higher susceptibility than given in [10]. The

experimental results at a high frequency of 23.5 Hz (see Fig. 7a in [10]) could not be found in our tested range of frequencies,  $0.01 \leq f \leq 0.5$ .

## 5 Summary

In order to describe the complex and nonlinear dynamics of a single peak of the Rosensweig instability in an oscillatory magnetic field, we propose a model aiming at an analytical equation for the height of the peak at its centre. Our model approximates the peak by a half-ellipsoid atop a layer of magnetic fluid. By exploiting the Euler equation for magnetic fluids and the analytical results for a rotational ellipsoid, we obtain a *nonlinear* equation for the dependence of the peak height on the applied induction (15). For static induction the quality of our proposed model is tested. It leads to the correct subcritical character of the bifurcation and gives the right width of the hysteresis compared with experimental results.

For a time-dependent induction the effects of inertia and damping are incorporated into equation (15). In correspondence with the experiments the dynamics is studied in a region, where the peak alternates between zero and a maximal height  $h_{max}$ . Our model shows not only qualitative agreement with the experimental results, as in the appearance of period doubling, trebling, and higher multiples of the driving period. Also a quantitative agreement is found for the parameter ranges of frequency and induction in which these phenomena occur.

For low frequencies the response of the peak is harmonic for nearly any strength of the external excitation which is a superposition of a static part and an oscillatory part. The whole area of harmonic response is cone-like shaped in accordance with the experiment. For a medium frequency a structure of periods is found, where a tongue of high periodic and non-periodic oscillations appears. For low values of the amplitude of the alternating induction, the tongue directly follows the period-1 state. For higher values of the amplitude the tongue is embedded in the period-2 state. The appearance and the location inside the parameter plane of an area of high periodic and non-periodic oscillations agree with the experimental data in the same frequency range.

Beside the agreement with the generic features observed in the experiment at low and medium frequencies, the model predicts a novel phenomenon. For a frequency of about 16.4 Hz the peak oscillates with the period  $N = 5$  as the final period before the oscillations between zero and  $h_{max}$  end (see Fig. 9b). It would be challenging to seek a final period greater than 2 in the experiment, because for the studied frequencies in [10] the final oscillations have only periods of  $N = 1$  or  $N = 2$ .

In the dynamics of a magnetic fluid with a low susceptibility a mixing of areas with different types of oscillations is found. For frequencies which are not too low, areas with oscillations between two positive extrema appear regularly inside areas with oscillations between zero and  $h_{max}$ . It would be interesting to test in experiments whether such a mixing can be observed for MF with low susceptibilities.

## Acknowledgment

The authors are grateful to Johannes Berg and René Friedrichs for helpful discussions. It is a pleasure to thank Andreas Tiefenau for providing the data of the shape of the magnetic fluid peak. This work was supported by the Deutsche Forschungsgemeinschaft under Grant EN 278/2.

## References

- [1] *Magnetic Fluids and Application Handbook*, edited by B. Berkovski and V. Bashtovoy (Begell House, New York, 1996).
- [2] R. E. Rosensweig, *Ferrohydrodynamics*, (Dover Publications, Mineola, 1997).
- [3] M. D. Cowley and R. E. Rosensweig, *J. Fluid Mech.* **30**, 671 (1967).
- [4] S. Sudo, M. Ohaba, K. Katagiri, and H. Hashimoto, *J. Magn. Magn. Mat.* **122**, 248 (1993).
- [5] M. Ohaba and S. Sudo, *J. Magn. Magn. Mat.* **149**, 38 (1995).
- [6] T. Mahr and I. Rehberg, *Phys. Rev. Lett.* **81**, 89 (1998).
- [7] J.-C. Bacri, U. d’Ortona, and D. Salin, *Phys. Rev. Lett.* **67**, 50 (1991).
- [8] V. G. Bashtovoi and R. E. Rosensweig, *J. Magn. Magn. Mat.* **122**, 234 (1993).
- [9] F. Elias, C. Flament, and J.-C. Bacri, *Phys. Rev. Lett.* **77**, 643 (1996).
- [10] T. Mahr and I. Rehberg, *Physica D* **111**, 335 (1998).
- [11] T. Mahr and I. Rehberg, *Europhys. Lett.* **43**, 23 (1998).
- [12] J. A. Stratton, *Electromagnetic Theory*, (McGraw-Hill, New York, 1941), p. 211-214 and 258. Equation (45) at page 214 has a misprint in a sign.
- [13] R. Richter, private communication.
- [14] J.-C. Bacri and D. Salin, *J. Phys. (France)* **45**, L559 (1984).

- [15] A. G. Boudouvis, J. L. Puchalla, L. E. Scriven, and R. E. Rosensweig, *J. Magn. Magn. Mat.* **65**, 307 (1987).
- [16] V. M. Zaitsev and M. I. Shliomis, *Sov. Phys. Dokl.* **14** 1001 (1970).
- [17] A. Engel, H. Lange, V. Chetverikov, *J. Magn. Magn. Mat.* **195**, 212 (1999); A. Engel, A. Lange, H. Langer, T. Mahr, M. Chetverikov, *J. Magn. Magn. Mat.* **201**, 310 (1999).
- [18] G. Matthies, to be published.
- [19] W. Chin, E. Ott, H. E. Nusse, and C. Grebogi, *Phys. Rev. E* **50**, 4427 (1994).
- [20] J. de Weger, D. Binks, J. Molenaar, and W. van de Water, *Phys. Rev. Lett.* **76**, 3951 (1996).

## Figures

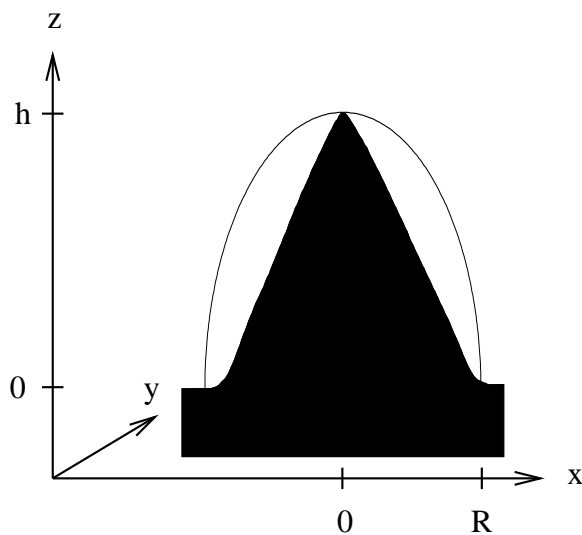


Fig. 1. Approximation of the MF peak by a half-ellipsoid with the vertical semiprincipal axis  $h$  and the horizontal semiprincipal axis  $R$ . The shape of the peak was measured in a setup used in [10] with the MF EMG 901 at  $B = 115.63 \cdot 10^{-4}$  T (courtesy of A. Tiefenau). The height of the peak is  $\sim 8.2$  mm.

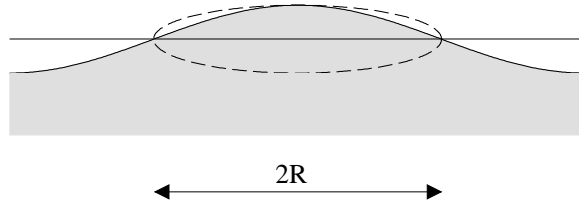


Fig. 2. Sketch of an ellipsoid inscribed into the crest of a sinusoidal surface wave with the wave length  $4R$ .

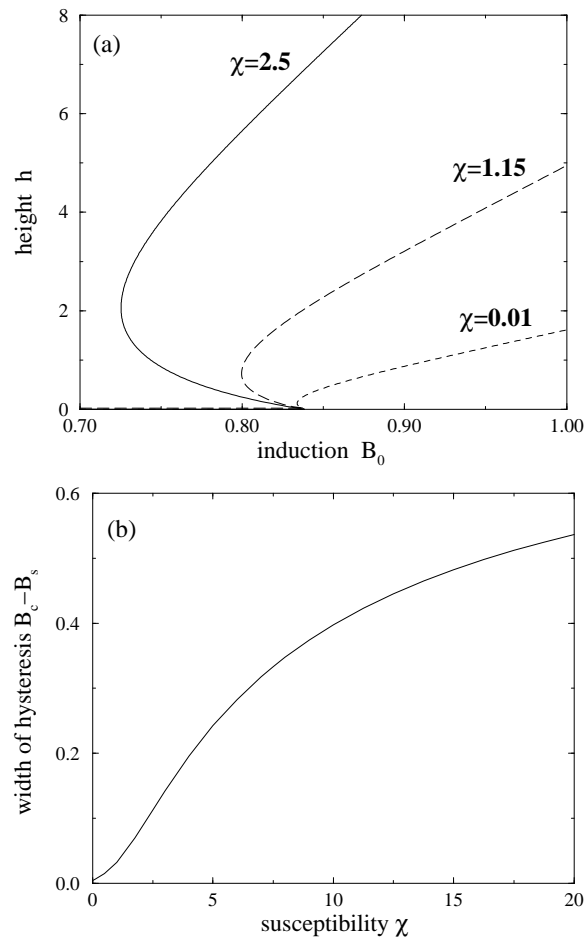


Fig. 3. (a) Height of the peak  $h$  versus the strength of the static external induction  $B_0$  as solution of Eq. (15) for  $\chi = 0.01$  (dashed line),  $\chi = 1.15$  (long-dashed line), and  $2.5$  (solid line). The critical induction for the subcritical bifurcation is independent of  $\chi$ , whereas the width of the hysteresis increases with increasing susceptibility. (b) The width of the hysteresis,  $B_c - B_s$ , is plotted versus the susceptibility  $\chi$  of the magnetic fluid.

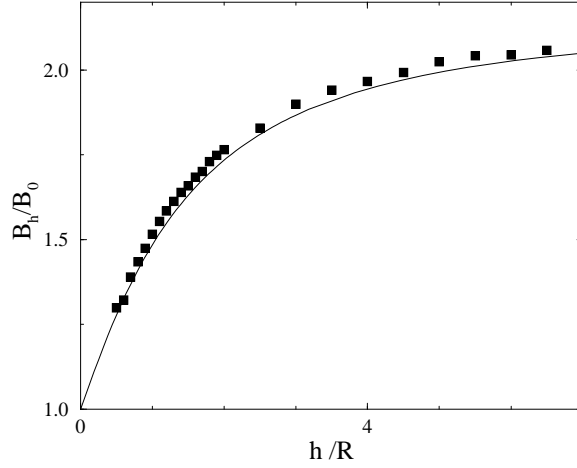


Fig. 4. The induction at the top of the peak  $B_h$  versus the height of of the peak  $h$ .  $B_h(h)$  is scaled with respect to the external static induction  $B_0$  (the radius of the half-ellipsoid  $R$ ). The solid line gives the solution of the approximation (10) with  $\lambda = -1/2$  and the filled squares indicate the results of the fully three-dimensional calculations [18] (courtesy of Matthies). The induction at the tip of the peak is approximated with an accuracy of 1.7%.

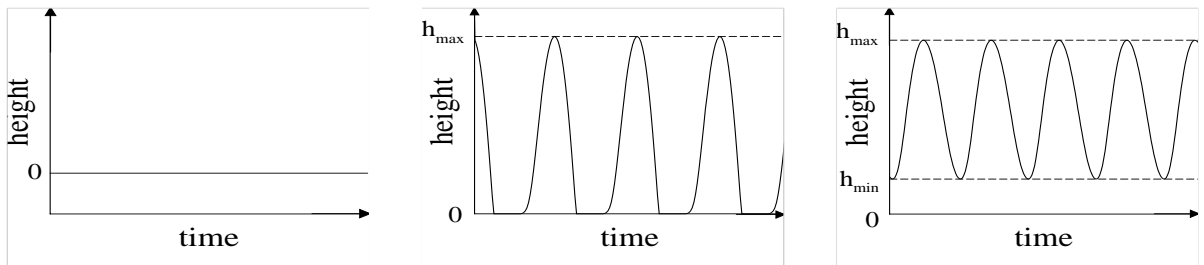


Fig. 5. Three different regimes for the temporal behaviour of the height of the peak at constant frequency and constant amplitude of the alternating part of the applied induction. For small values of the static induction the height is zero (left), for moderate strengths the height oscillates between zero and a maximum (middle), and for large values the height alternates between a minimum and maximum both larger than zero (right). Only the second regime is analysed in detail.

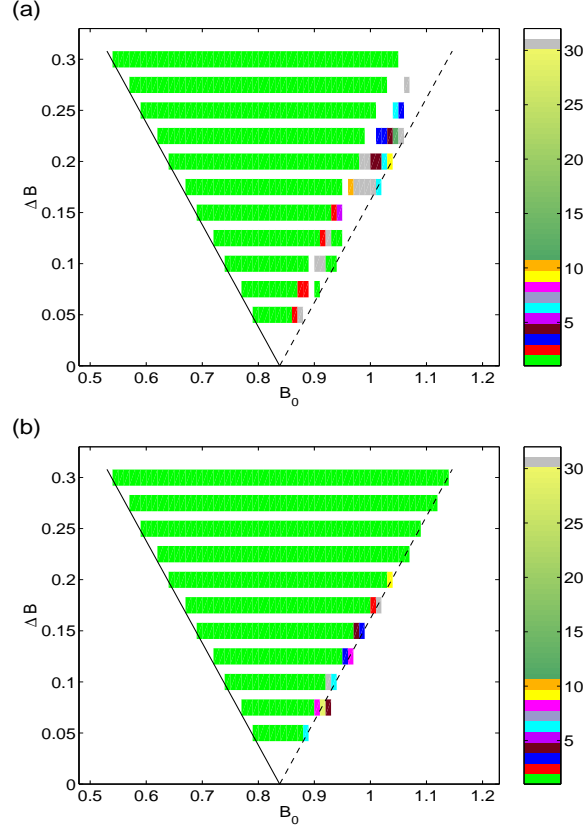


Fig. 6. Periods of the peak oscillations in dependence of the static induction  $B_0$  and the amplitude of the alternating induction  $\Delta B$  at a small frequency of  $f = 0.03$  ( $\simeq 2.5$  Hz) for the susceptibilities  $\chi = 1.15$  (a) and  $\chi = 2.5$  (b). The peak oscillates harmonically almost everywhere in the  $B_0$ - $\Delta B$  plane. The area of harmonic response is cone-like shaped. The limit to the left is given by  $\Delta B = B_c - B_0$  for  $B_0 \leq B_c$  (solid line) and the limit to the right is given by  $\Delta B = B_0 - B_c$  for  $B_0 \geq B_c$  (dashed line). Slight deviations from these features appear for  $\chi = 1.15$  (a). The colour code for the periods 1 to 30 is given in the legend. Periods above 30 and non-period behaviour are displayed in grey.

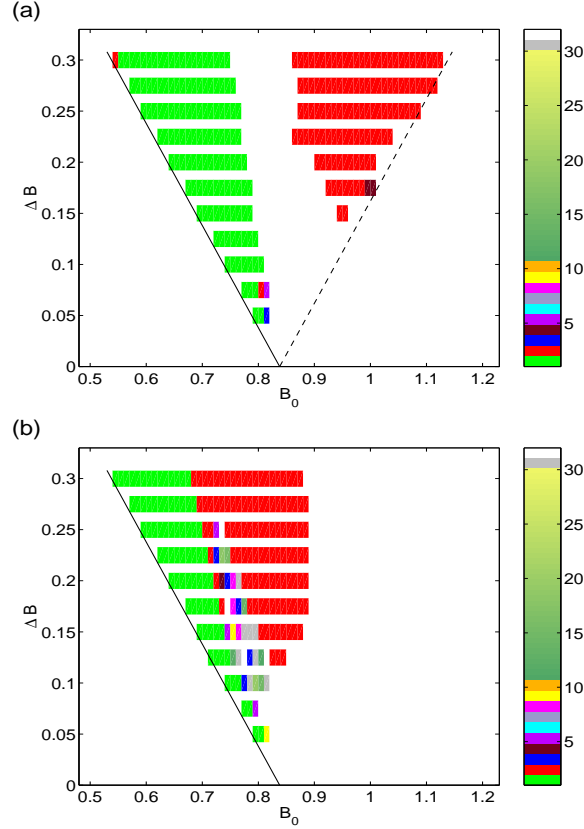


Fig. 7. Periods of the peak oscillations in dependence of the static induction  $B_0$  and the amplitude of the alternating induction  $\Delta B$  at a medium frequency of  $f = 0.1$  ( $\simeq 8.2$  Hz) for the susceptibilities  $\chi = 1.15$  (a) and  $\chi = 2.5$  (b). (a) Two disjoint parts appear, where for smaller values of  $B_0$  the peaks oscillates harmonically and for higher values of  $B_0$  the period-2 state emerges. (b) For high amplitudes  $\Delta B$  harmonic oscillations and period doubling are only present. For smaller amplitudes of  $\Delta B$  a tongue of high periodic ( $2 < N < 19$ ) and non-period oscillations appears. The solid line indicates  $\Delta B = B_c - B_0$  for  $B_0 \leq B_c$  and the dashed line marks  $\Delta B = B_0 - B_c$  for  $B_0 \geq B_c$ . The colour code for the periods 1 to 30 is given in the legend. Periods above 30 and non-period behaviour are displayed in grey.

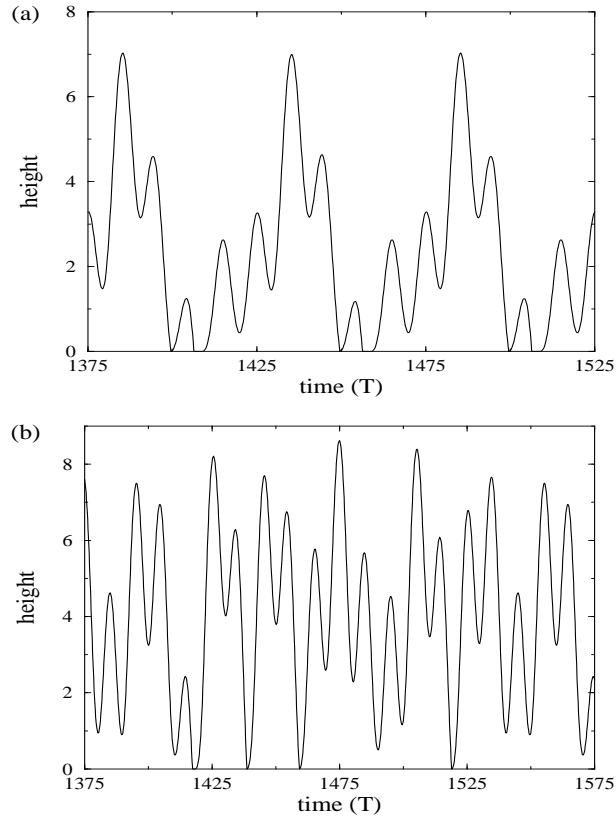


Fig. 8. Oscillations of the height of the peak with a period  $N = 5$  (a) and  $N = 16$  (b) at a driving frequency of  $f = 0.1$  ( $\simeq 8.2$  Hz) for a MF with a susceptibility of  $\chi = 2.5$ . The other parameters are: (a)  $\Delta B = 0.15$  and  $B_0 = 0.74$ , (b)  $\Delta B = 0.225$  and  $B_0 = 0.74$ . Note the different scales at the axes.

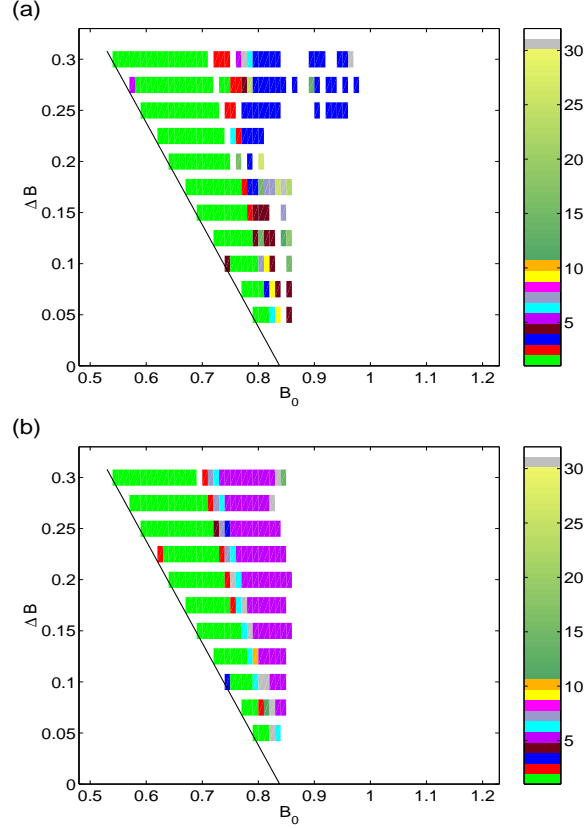


Fig. 9. Periods of the peak oscillations in dependence of the static induction  $B_0$  and the amplitude of the alternating induction  $\Delta B$  at a frequency of  $f = 0.2$  ( $\simeq 16.4$  Hz) for the susceptibilities  $\chi = 1.15$  (a) and  $\chi = 2.5$  (b). (a) The peak starts to oscillate harmonically independent of the strength of  $\Delta B$ . With increasing  $B_0$  the period-1 state is followed by a period of  $N = 4$  (small  $\Delta B$ ) or  $N = 2$  and 3 (large  $\Delta B$ ). (b) The whole period diagram displays a band-like structure formed by areas of period  $N = 1, 2, 5,$  and  $6$ . The solid line indicates  $\Delta B = B_c - B_0$  for  $B_0 \leq B_c$ . The colour code for the periods 1 to 30 is given in the legend. Periods above 30 and non-period behaviour are displayed in grey.

